2.5 SHIPBOARD TURBULENCE MEASUREMENTS OF THE MARINE ATMOSPHERIC BOUNDARY LAYER FROM HIRES EXPERIMENT

John Kalogiros[1*], Q. Wang[2], R. J. Lind[2], T. Herbers[2], and J. Cook[2]
[1]National Observatory of Athens, Athens, Greece
[2]Naval Postgraduate School, Monterey, California

1. INTRODUCTION

The High Resolution Air-Sea Interaction (HiRes) DRI main experiment (1 to 30 of June, 2010) took place near the north to central California coast offshore Bodega Bay (Fig. 1). In-situ and sodar turbulence measurements were collected onboard R/V Robert Gordon Sproul (about 35 m length and 9.5 m maximum height).

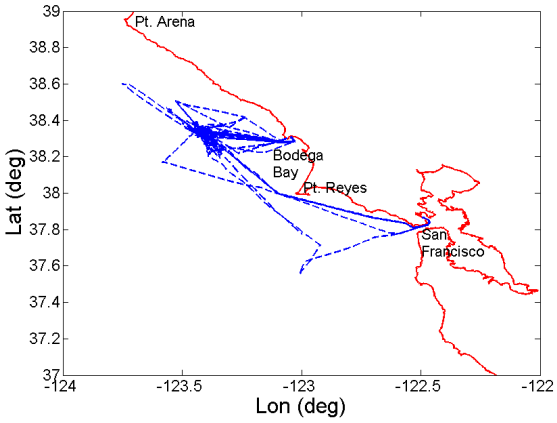

Figure 1. Ship track during HiRes experiment.

In-situ instruments were installed on 12 m high masts at the bow (bow mast) and the crow nest (middle of the ship, ship mast). The principal sensors installed on each mast were: CSAT-3 sonic anemometer and a CS7500 - LiCor LI7500 open path H_20/CO_2 analyzer/hygrometer. The bulk meteorology sensors were mean temperature and humidity sensors in aspirator and 2-D sonic anemometers for mean wind. Data of platform motion due to ship movement and sea waves was obtained with a fast TNT compass and tilt meter, MotionPak II accelerometer and angular rates meter and a GPS receiver for correction of wind data similar to Edson et al. (1998). Data was logged at 20 Hz sampling rate with a CR5000 data logger and transferred to a notebook PC periodically. The mast at the bow of the ship was forward inclined at an angle of 15 to 20 degrees off the vertical towards the front of the ship. Flow distortion by the ship superstructure at the ship mast was evident for turbulence (higher turbulence, i.e. generation of turbulence) and less for wind speed (an example is given in Fig. 2). Thus, bow mast data were used in the analysis.

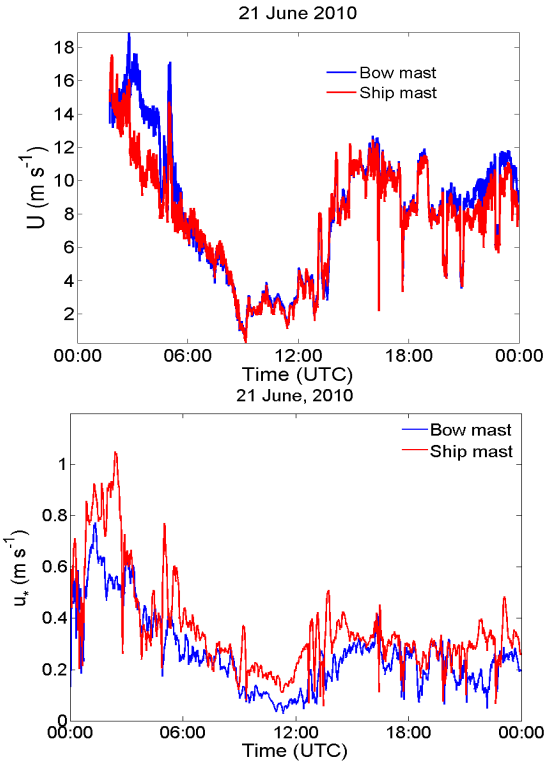

Figure 2. Measured wind speed (U) and friction velocity (u_*) at the two masts on June 21, 2010.

A Doppler minisodar from Atmospheric Science Corporation (acoustic frequency 4.5 kHz) was installed at the back and near the side of the ship. The nominal range of the sodar was 250 m with a vertical resolution of 5 m (gate length). The system transmits a pulse about every 1.5 s sequentially in one vertical and two inclined at 16 degrees off the vertical direction (beams) and measures the intensity and Doppler spectrum of the backscattered signal. Thus, wind vector estimates were obtained in 5 sec time periods. Turbulence was also recorded with high vertical resolution (1.7 m) as thermal turbulence (temperature small scale variations) which corresponds to the intensity of

* *Corresponding author address:* John Kalogiros, National Observatory of Athens, 15236, Athens, Greece; e-mail: jkalog@noa.gr.

backscattered acoustic signal. Due to significant ship motion and tilt correction of sodar Doppler velocities was required and, thus, an additional motion detection system similar to the one installed on the meteorological masts was used. The sampling rate for this motion detection system was 10 Hz.

In the next sections results from the corrected for ship motion and processed turbulence mast data, Coupled Ocean Atmosphere Mesoscale Prediction System (COAMPS) mesoscale model and sodar data are presented. The mast data are used to check the effect of wave parameterizations on turbulent transfer coefficients (mainly drag coefficient), while results from operational COAMPS simulations are validated against mast data. Sodar data is shown to be useful to study the vertical turbulence structure in the marine boundary layer and a preliminary validation against mast data is given here.

2. WAVE EFFECTS ON TURBULENT TRANSFER COEEFICIENTS

Sea surface wave data were collected during the experimental period with a moored DWR-G7 directional waverider Datawell buoy of NPS. The sea depth at its position was 157 m (i.e., deep waters). The buoy samples horizontal (north, west) and vertical displacements were recorded continuously at 1.28 Hz. Power and cross spectra were computed using the Fourier transform in segments of 256 samples with 50 % overlap and a Hamming window. The wave directional spectrum was estimated with Longuet-Higgins method. Figure 3 show an example of wave spectrum from this buoy. The peaks and directions of swell (large wave periods) and locally wind generated sea waves (short wave periods) are evident. The wind speed U and direction from the bow mast of the ship were used to separate wave frequencies in swell and sea waves. Wind sea waves were identified as the wave spectrum peak with direction difference Δdir between wind and waves less than 45 degrees, and a wave phase velocity C_p<1.3Ucos(Δdir) according to Drennan et l. (2003). The wave spectrum was characterized as sea waves if the wave energy of sea waves E_{sea} was higher than the energy E_{swell} of swell waves. A more strict criterion for swell definition is also used in literature is E_{swell}>5E_{sea}. In this work the balance between swell and sea wave energy was used, which separated better the two wave categories in the current data. Swell cases were less frequent (30% of total data) than wind sea waves and their majority was swell following wind (i.e., in the same direction) from NNW.

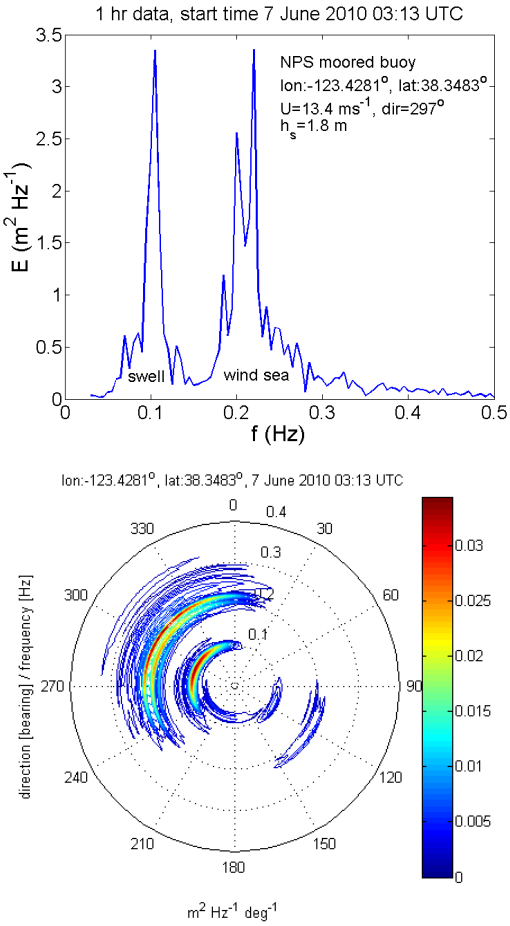

Figure 3. Power and directional wave spectrum from NPS buoy with identification of swell and sea waves on June 7, 2010.

Figure 4 shows also the cyclic frequency of the sea waves peak (ω_p) versus the expected frequency of mature (saturated, well developed) sea waves g/1.3Ucos(Δdir) (Kraus and Businger 1994). The frequency of deep waters waves is g/C_p and, thus, the saturation line is the limit where the phase speed of waves C_p becomes equal to the maximum possible value of 1.3Ucos(Δdir). The ratio C_p/ Ucos(Δdir) is a definition of the wave age and young waves have small wave age (i.e., they have not reached saturation). The majority of data points are away from the saturation line, which means that the sea waves were young sea waves. Thus, wave height and period estimation (for example in parameterizations of turbulent fluxes and air-sea coupling models) using mature wave relationships may fail under these conditions.

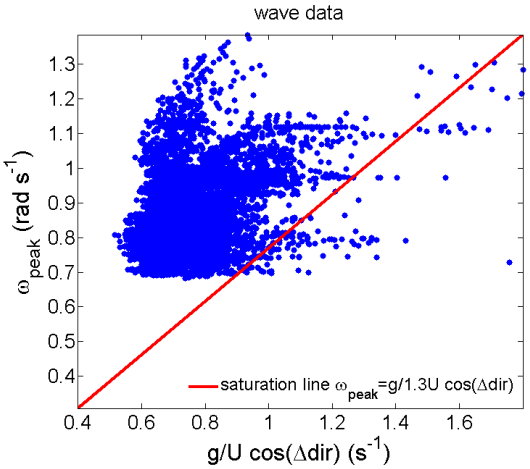

Figure 4. Cyclic frequency of the sea waves peak (ω_p) versus the expected frequency of mature (saturated, well developed) sea waves.

Sea surface waves affect the turbulent transfer coefficients mainly through their effect on the velocity roughness length. The parameterizations of velocity roughness length z_{0u} examined in this study are summarized below:

$$z_{0u}=0.011u_*^2/g+0.11v/u_*, \quad (1)$$

$$z_{0u}=50(u_*^2/g)\,(u_*/C_p)^{2.5}+0.11v/u_*, \quad (2)$$

$$z_{0u}=1200h_s(h_s/L_p)^{4.5}+0.11v/u_*, \quad (3)$$

$$z_{0u}=1.7(u_*^2/g)(u^*/C_p)^{1.7}+0.11v/u_*, \quad (4)$$

$$z_{0u}=13.4(h_s/4)(u_*/C_p)^{3.4}+0.11v/u_*, \quad (5)$$

where the smooth flow limit is $0.11v/u_*$ (v is the kinematic viscosity of air and u_* is the friction velocity). Equation (1) is the classic Charnock formula presented by Charnock (1955) and followed by Fairall et al. (1996), while Eqs. (2)-(5) are based on empirical wind sea wave data according to Oost et al. (2002) Eq. (2), Taylor and Yelland (2001) Eq. (3), and Drennan et al. (2003) Eqs. (4) and (5). The significant wave height h_s (defined as $4E^{1/2}$, E is the wave energy calculated by integration of the wave power spectrum) and the time period T_p (L_p wavelength, $C_p=L_p/T_p$ is the phase speed) of the wave spectrum peak for mature sea waves were also estimated according to Taylor and Yelland (2001):

$$h_s=0.0248U^2 \quad (6)$$

$$T_p=0.729U. \quad (7)$$

The ratio h_s/L_p is the wave slope or steepness, and C_p/u_* is a definition of wave age based on u_* which connects wave parameters with the direct cause (wind stress) of waves. The above parameterizations apply to sea waves and do not include swell effects. Thus, in time periods when swell is present and its energy dominates over sea waves these parameterizations are expected to fail.

In the results presented only ship data with a head wind (within 30 degrees from ship heading) was used in order to avoid possible flow distortion by the ship superstructure. About 7000 data points were selected out of about 32000 points. Each data point corresponds to 10 minutes time periods with 1 minute shift, i.e. 9 minutes overlap. The wind bins are 1 m s^{-1} (bins with less than 10 data points in the bin were excluded). The range of values of the last bin is 17 to 18 m s^{-1}, which includes the maximum observed 10 minutes average wind speed. In addition, noisy values of the sensible heat flux transfer coefficient C_h were manually detected from its time series and removed (about 1000 data points were finally selected).

Figure 5 shows neutral drag coefficients C_{dn} from bow mast against neutral wind speed using the above parameterizations of velocity roughness length. The reduction of data to neutral stability values and 10 m height above mean sea level was made according to Kalogiros and Wang (2011) using surface layer relations. The results from COARE 3.0 bulk parameterization of turbulent fluxes (Fairall et al. 2003), which is used in many mesoscale atmospheric models, with the corresponding parameterization of velocity roughness length are also presented. Scalar (sensible and latent heat) roughness lengths were estimated similar to COARE using the LKB parameterization of Liu et al. (1979) which is based on the roughness Reynolds number $R_r=z_{0u}u_*/v$. The term "wave estimation" in figures corresponds to estimation of wave parameters (h_s and T_p) from the above empirical relations Eqs. (6) and (7) instead of actual wave data. Data are also separated in swell and sea waves cases according to the wave energy criterion mentioned above.

According to Fig. 5 changes in C_{dn} are significant for different z_{0u} parameterization. The drag coefficients estimated from COARE follow very well the measured values when the estimation of the velocity roughness length from Eq. (3) is used. The data with very high swell effects (usually at very low wind speed) do not follow COARE, which is expected because such effects are not included in the parameterizations.

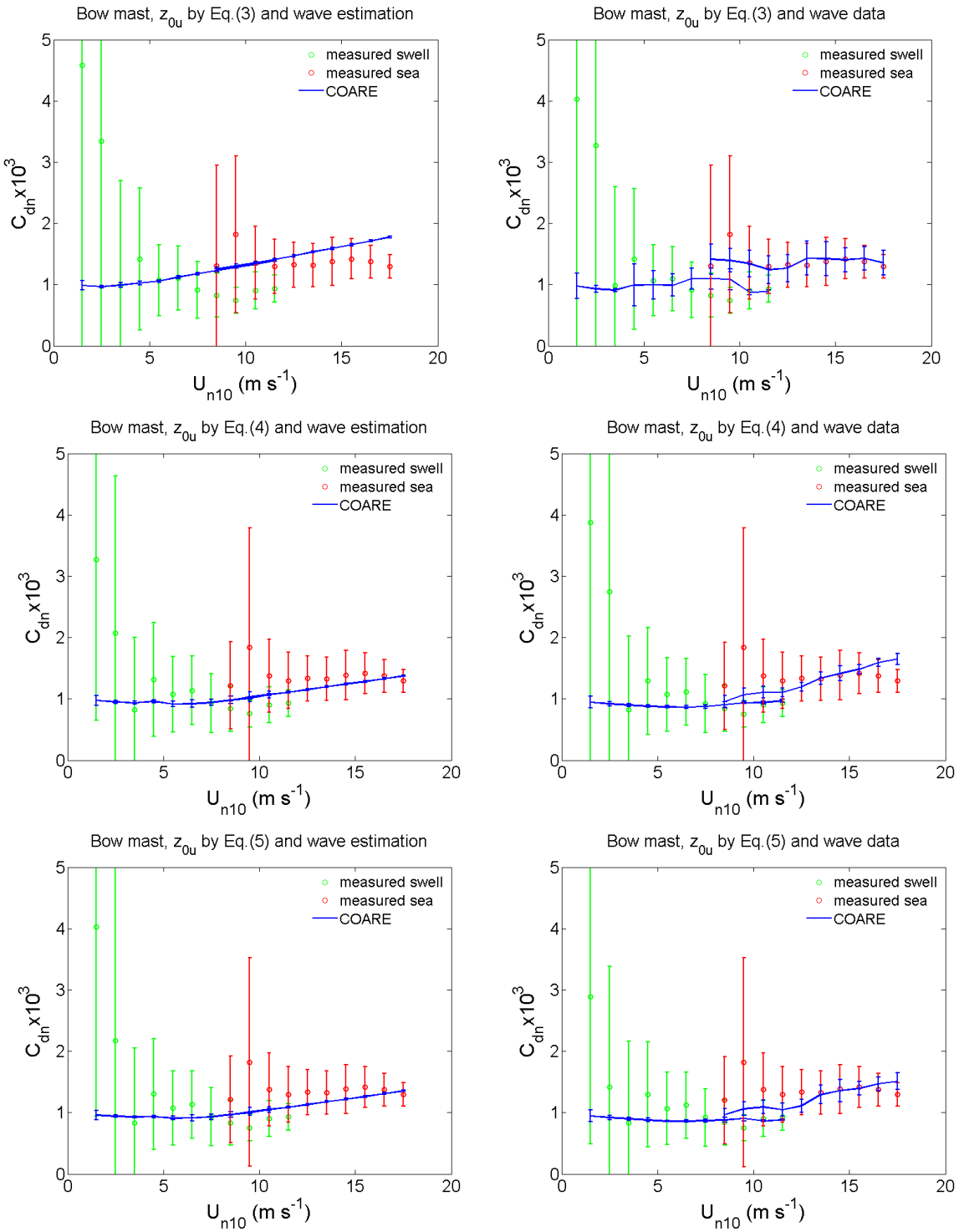

Figure 5. Neutral drag coefficient C_{dn} against neutral wind speed at 10 m above sea level U_{n10} in wind bins of 1 m s^{-1} with standard deviation and with z_{0u} estimated from Eqs. (3), (4) and (5).

Eq. (3) is based on wave parameters (h_s and L_p) and specifically the wave steepness (h_s/L_p) without including the friction velocity and, thus, its success could probably be expected. However, sea waves observed during the experiment were young waves as shown in Fig. 4 and the estimation of wave parameters, which is based on mature sea relations, fails. Thus, Eqs. (4) and (5) are more successful if actual wave data is not available or not forecasted with a wave model.

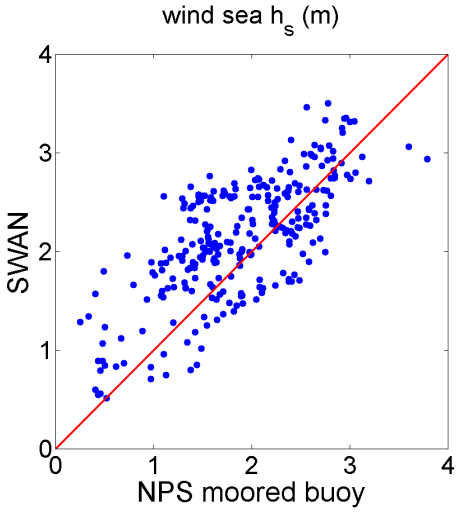

Figure 6. Scatter plot of SWAN significant wave height h_s against buoy measurements.

Wave models could give forecasts of wave characteristics and combined with atmospheric models like COAMPS. Thus, in order to check this argument forecasts from a wave model were compared with wave measurements by NPS buoy. Figure 6 shows the comparison of Simulating Waves Nearshore (SWAN) wave model forecasts with buoy data for significant wave height. The SWAN wave forecasts used are from 12 to 24 hours ahead of analysis time in the time period of the experiment. The resolution of SWAN nest that was used was 4.5 to 5.5 km. The results from SWAN were for the wind sea part of wave spectrum. Thus, swell periods were excluded from the comparison. The agreement of forecasts with measurements is good on average. However, the scatter of the comparison for significant wave height is about 0.5 m, which is relatively high (25% at 2 m value), and there is small trend for SWAN to overestimate it.

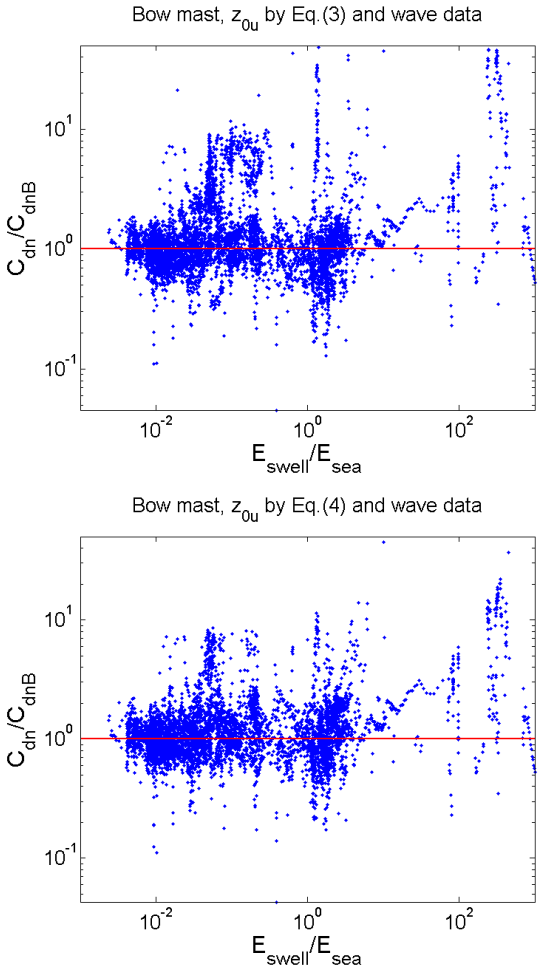

Figure 7. Ratio of measured C_{dn} to COARE C_{dnB} neutral drag coefficient versus the ratio of swell to sea wave energy using Eqs. (3) and (4) for z_{0u}.

In order to evaluate the effect of swell on the drag coefficient the ratio of measures to COARE estimated coefficient C_{dnB} is presented in Fig. 7 against the observed ratio of swell to sea wave energy. Raw data instead of wind bin averages are shown in order to show all data including outliers. The clear swell cases with $E_{swell}>5E_{sea}$ are limited, but still the trend of measured drag coefficient for increasing values with swell energy is clear. The same behavior was as also observed in aircraft data by Kalogiros and Wang (2011). For sea waves the results from the application of Eq. (3) with actual wave data show the smaller bias and dispersion around unity of the corresponding ratio between observations and COARE estimation. Sea waves data with high observed drag coefficients (ratio higher than 3) is due to problems in the ship data during some time

periods and non-convergence of the algorithm for reduction to neutral drag coefficient.

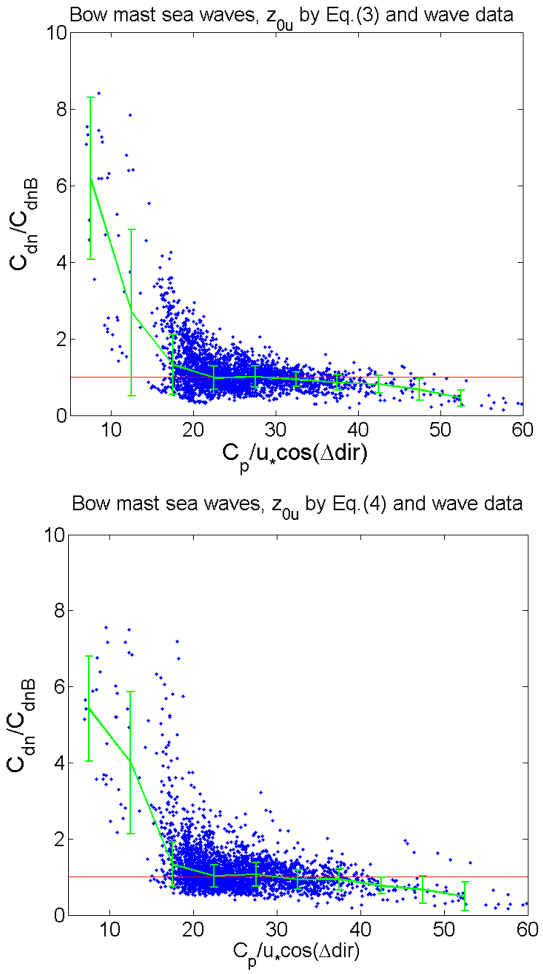

Figure 8. Ratio of measured to COARE neutral drag coefficients against sea wave age with z_{0u} estimated from Eqs. (3) and (4).

Figure 8 shows the ratio of measured to COARE neutral drag coefficients against wave age estimated using friction velocity with velocity roughness length estimated from Eqs. (3) and (4) for the cases of wind sea waves. Young waves are characterized by quite higher drag coefficient values, while old waves are characterized by lower values compared to the bulk COARE parameterization. In the range of wave age values from about 20 to 40 the parameterizations are satisfactory especially when measured wave parameters are used. It should be noted that Eq. (4), which includes wave age, also does not produce good results out of this range of wave age values. This could probably be expected because the parameterizations have been developed mainly with wave data with wave age in this range.

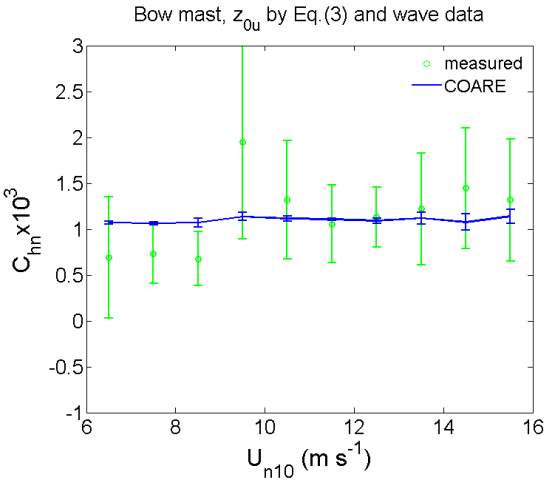

Figure 9. Neutral sensible heat transfer coefficient C_{hn} from bow mast data against neutral wind speed at 10 m above sea level with z_{0u} estimated from Eq. (3) and measured wave parameters.

Figure 9 shows neutral the heat transfer coefficient estimated from bow mast data. There is good agreement with COARE estimations and the wave effect on this coefficient is small, so that there is little difference in the coefficients when wave data instead of wave estimation is used. Turbulence measurements from ship mast (not shown here) presented turbulent transfer coefficients quite higher than COARE estimations, which is an indication that those measurements were significantly affected by the superstructure of the specific ship.

3. VALIDATION OF COAMPS FORECASTS

In this section preliminary results from the comparison of COAMPS mesoscale model results with the ship measurements of wind and momentum flux are shown. The resolution of COAMPS nest which was used was 3 km. The parameterization of surface fluxes in COAMPS follows Louis (1979) scheme, which uses polynomial functions of the bulk Richardson number to directly compute surface sensible heat flux, surface latent heat flux, and surface drag. Surface roughness is obtained by Eq. (1). There is also an option to use COARE algorithm, but it is turned off by default.

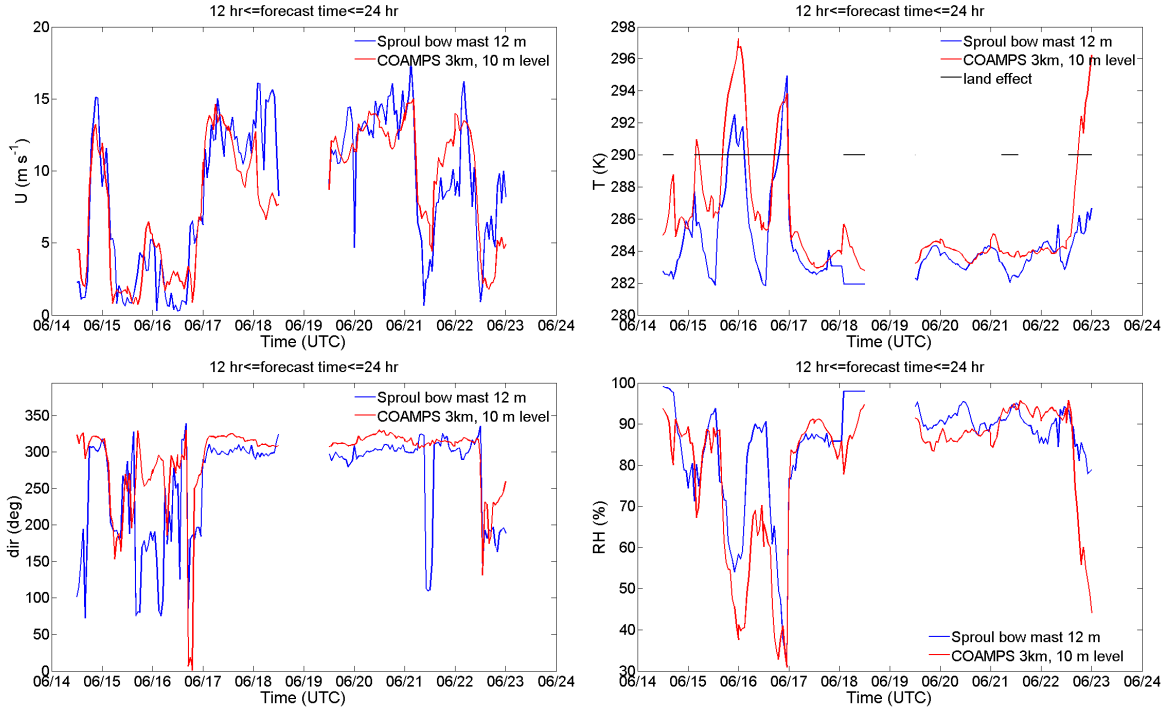

Figure 10. Time series of COAMPS forecasted and bow mast measurements of wind speed (U) and direction (dir), air temperature (T), and relative humidity (RH).

Figure 10 shows time series of the COAMPS near surface forecasts from 12 to 24 hours ahead of analysis time in the time period 14 to 24 June, 2010 when there was a long time period of continuous ship observations. The agreement of COAMPS forecast with bow mast measurements of wind speed and direction for this time period is satisfactory. The bias of COAMPS forecast in the wind direction is about 10 degrees. In time periods that the ship was near coast (less than 10 km distance) COAMPS forecasts (especially temperature) were affected significantly by model resolution at the land-sea border. Ship data also showed a similar land effect when the ship was getting close to port. Thus, in addition to the selection criteria for ship data mentioned in section 2 data with this land effect were not included in the comparison of COAMPS forecasts with ship measurements.

The agreement of COAMPS forecast of wind speed and direction with mast measurements of wind speed and direction presented in Fig. 11 is satisfactory in qualitative terms. However, the comparison of wind components COAMPS (not shown here) shows that COAMPS presents a negative bias of north component and a positive bias for east component. Figure 12 shows the scatter plot for friction velocity, which indicates a small general trend for COAMPS to overestimate friction velocity mainly due to the wind speed differences as mentioned above. The drag coefficient comparison shows that on average the parameterization used by COAMPS follows well the measurements but there is significant scatter. Also, the wind speed range is relatively small and the trend with wind speed is not clear in measurements. Heat fluxes were very small over sea (away from land) and, thus, a comparison for heat fluxes over sea was not possible.

4. SODAR MEASUREMENTS

Sodar (Sonic Detection And Ranging) is a remote acoustic sensing system able to detect low level turbulence in the marine boundary layer. There are many measurement problems operating a sodar on a ship and these are mainly engine and environmental (wind generated) noise and sound reflection and ship motion. The noise and reflection problem was partially controlled by installation at the back area of the ship, but still limited the maximum range of measurements to about 200 m and many noisy measurements were present in the data. The effect of the motion of ship was also mostly removed using motion and attitude data from a navigation system similar with

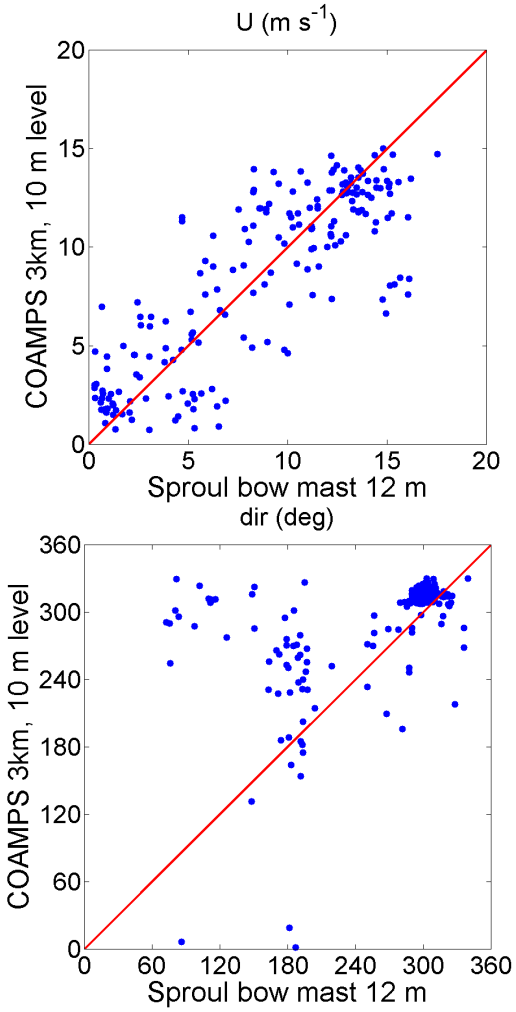

Figure 11. Scatter plots of COAMPS wind speed (U) and direction (dir) against ship measurements.

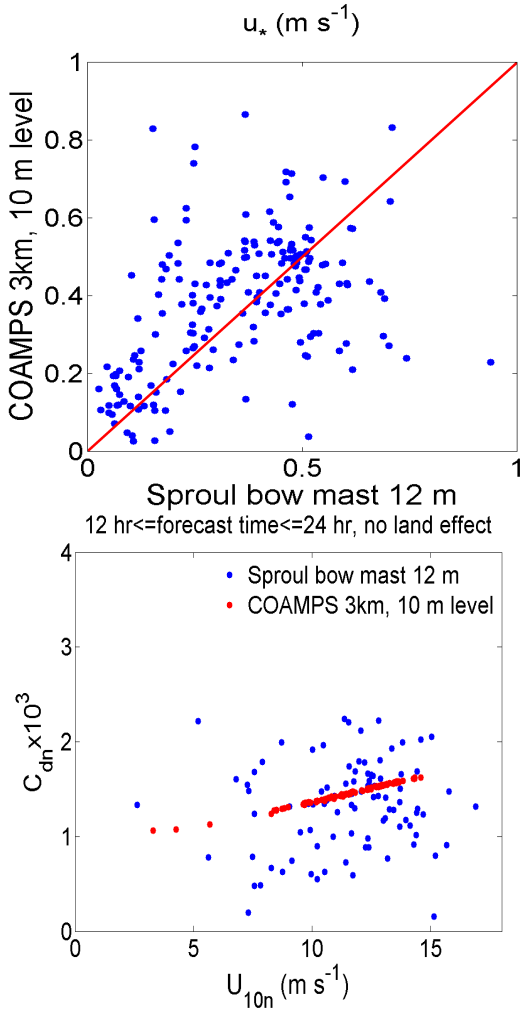

Figure 12. Scatter plots of COAMPS friction velocity u_* against ship measurements and neutral drag coefficient C_{dn} against wind speed U reduced to 10 m above sea surface and neutral conditions.

the ones installed on the masts, but still during high oscillations due to high winds and sea waves the backscattered acoustic signal does not reach the sodar antenna and, thus, the range of measurements is decreased even more.

Figure 13 show time-height plots of sodar measurements of wind speed and direction and vertical velocity variance on two days. Due to sound reflection by the ship sodar does not give reliable measurements in about the first 20 m above its antenna and, thus, a direct comparison with mast data is not possible. However, comparing sodar data with mast data (Fig. 14) it can be seen that the sodar follows well the intensity and variation of wind speed and direction from high wind to low wind speed with significant turn of direction on 21 June, 2010. The vertical velocity variance, which is a measure of vertical velocity variance, which is a measure of turbulence, follows the daily trend observed in mast data with low values in the middle of the 21st of June (Fig. 2). Vertical velocity variance and monetum flux (not shown here) values by the sodar are higher from bow mast values due to the inclusion of noisy measurements despite the rejection of data with bad signal to noise ratio despite quality control checks of sodar data. However, sodar records layers of elevated turbulence (Fig. 13) can reach 200 m above sea surface (vertical structure of turbulence).

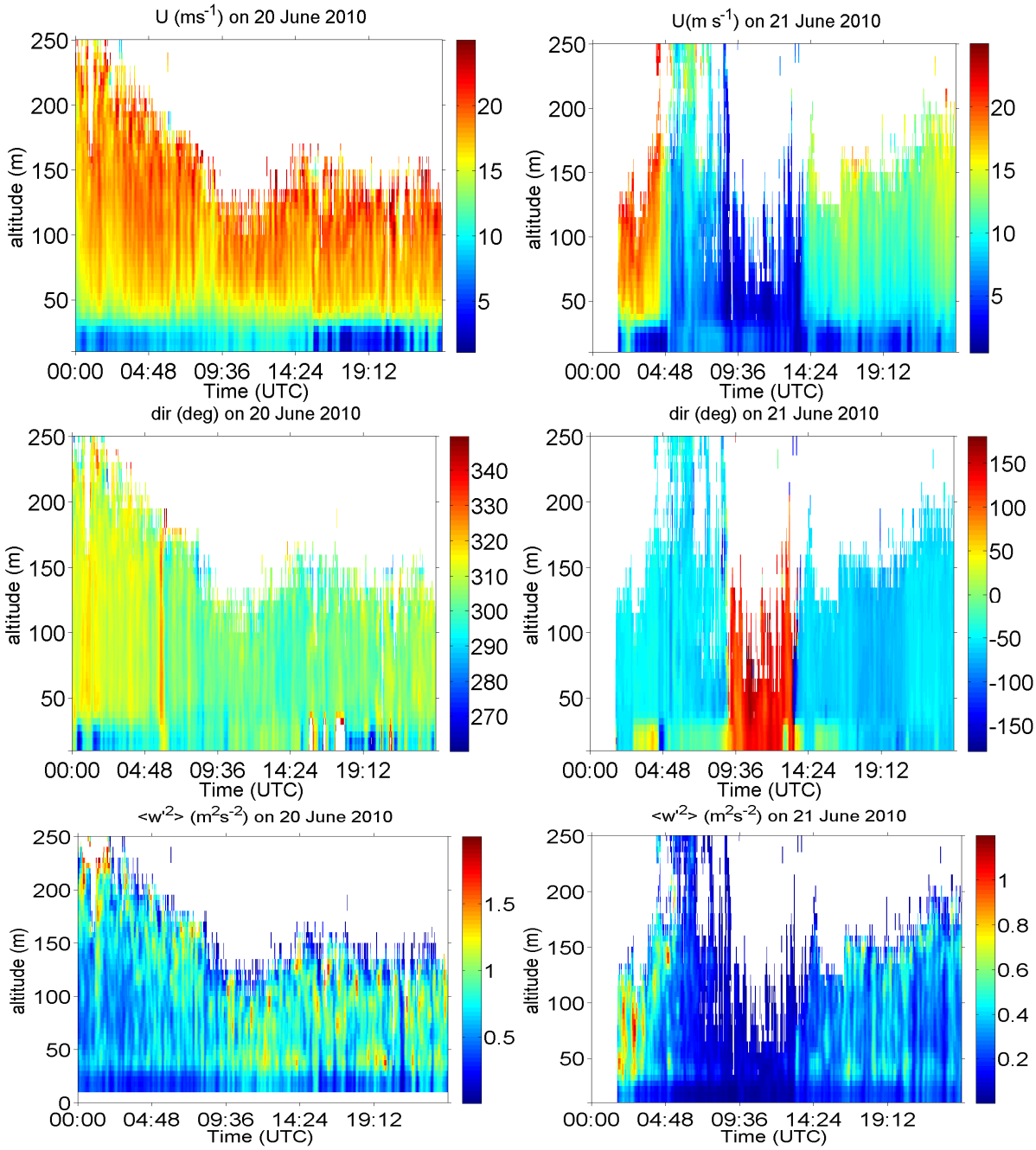

Figure 13. Sodar wind speed (U) and direction (dir) and vertical velocity variance $\langle w^2 \rangle$ along mean wind direction (10 minutes averaging) on 20 and 21 of June, 2010.

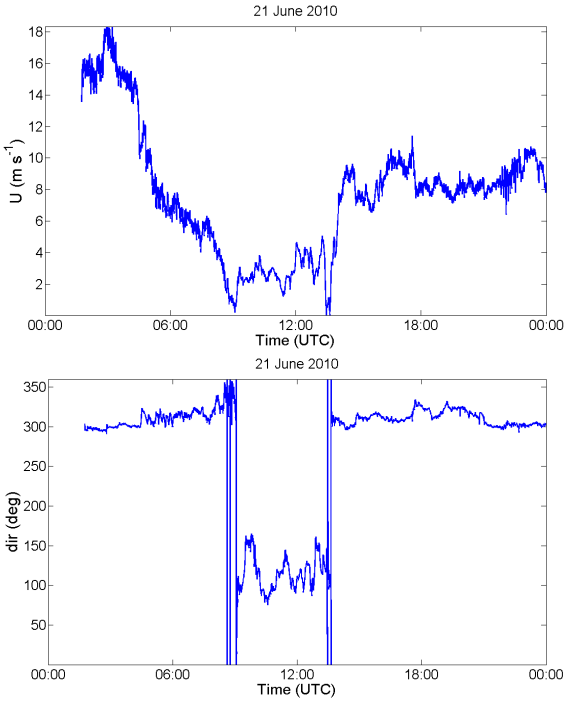

Figure 14. Wind speed U and direction dir (10 minutes averaging) from bow mast on 21 of June, 2010.

6. CONCLUSIONS

Turbulence data were collected during the HiRes main experiment aboard R/V Sproul in June, 2010 offshore of Bodega Bay, California. Although two sets of measurements were made from the bow mast and the ship center mast, data from the bow mast were used because this position was found to be least affected by flow distortion due to the ship superstructure. Waves during the experiment were mainly non-saturated waves generated locally by wind (wind sea waves) and swell waves were less frequent.

Combined with in situ wave measurements, the sea-state dependent surface flux parameterizations were studied using this dataset by examining the effects of wind sea waves on turbulent transfer coefficients through the velocity roughness length. A comparison of various parameterizations showed that the formulation based on wave steepness gave the best results for the current dataset. However when wave data is not available and are estimated from relations for mature wind sea wave parameterizations which use wave age (i.e. wind speed or wind stress information) are satisfactory. Another option is to estimate wave parameters from a wave forecast model like SWAN. Also, young wind sea waves as well as swell were characterized by high drag coefficients, which are not explained by the current parameterizations. Forecasts from COAMPS atmospheric model at the position of the ship were also compared with measurements and showed reasonable agreement for wind speed, wind direction, and friction velocity. The discrepancies between the forecast and observations of friction velocity were mainly due to the corresponding differences in wind speed. Concurrent sodar measurements showed the existence of turbulence structures up to 200 m above sea level and the sodar estimated wind and momentum flux followed qualitatively the variations of corresponding mast observations.

ACKNOWLEDGEMENTS

This work is sponsored by the Office of Naval Research (ONR) award No. N0001409WR20059.

REFERENCES

Charnock, H., 1955: Wind stress on a water surface. *Quart. J. Roy. Meteorol. Soc.*, **81**, 639-640.

Drennan, W.M., H.C. Grabe., D. Hauser, and C. Quentin, 2003: On the wave age dependence of wind stress over pure wind seas. *J. Geophys. Res.*, **108**, 8062-8074

Edson, J.B., A.A. Hinton, K.E. Prada, J.E. Hare, and C.W. Fairall, 1998: Direct covariance flux estimates from mobile platforms at sea. *J. Atmos. Oceanic Technol.*, **15**, 547-562.

Fairall, C.W., E.F. Bradley, D.P. Rogers, J.B. Edson, and G.S. Young, 1996: Bulk parameterization of air-sea fluxes for tropical ocean-global atmospheric coupled-ocean atmospheric response experiment. *J. Geophys. Res.,* **101**, 3747-3764.

Fairall, C.W., E.F. Bradley, J.E. Hare, A.A. Grachev, and J.B. Edson, 2003: Bulk parameterization of air-sea fluxes: Updates and verification for COARE algorithm. *J. Clim.*, **16**, 571-591

Kalogiros, J.A., and Q. Wang, 2011: Aircraft observations of sea-surface turbulent fluxes near the California coast. *Boundary-Layer Meteorol.* **139**, 283-306.

Kraus, E.B., and J.A. Businger, 1994: Atmosphere-Ocean Interaction. Oxford University Press, New York, 362 pp

Liu, W.T., K.B. Katsaros, and J.A. Businger, 1979: Bulk parameterization of the air–sea exchange of heat and water vapor including the molecular

constraints at the interface. *J. Atmos. Sci.,* **36**, 2052–2062

Louis, J.F., 1979: A parametric model of vertical eddy fluxes in the atmosphere. *Boundary-Layer. Meteorol.,* **17**, 187-202.

Oost, W.A., G.J. Komen, C.M.J. Jacobs, and C. Van Oort, 2002: New evidence for a relation between wind stress and wave age from measurements during ASGAMAGE. *Boundary-Layer Meteorol.*, **103**, 409-438

Taylor, P.K., and M.J. Yelland, 2001: The Dependence of Sea Surface Roughness on the Height and Steepness of the Waves. *J. Phys. Oceanogr.,* **31**, 572-590